fractal and fractional

MDPI

Article

A Numerical Algorithm for Solving Nonlocal Nonlinear Stochastic Delayed Systems with Variable-Order Fractional Brownian Noise

Behrouz Parsa Moghaddam [1], Maryam Pishbin [1], Zeinab Salamat Mostaghim [1], Olaniyi Samuel Iyiola [2], Alexandra Galhano [3,*] and António M. Lopes [4]

[1] Department of Mathematics, Lahijan Branch, Islamic Azad University, Lahijan 1477893855, Iran
[2] Department of Mathematics, Clarkson University, Potsdam, NY 13699, USA
[3] Faculdade de Ciências Naturais, Engenharias e Tecnologias, Universidade Lusófona do Porto, Rua Augusto Rosa 24, 4000-098 Porto, Portugal
[4] LAETA/INEGI, Faculty of Engineering, University of Porto, Rua Dr. Roberto Frias, 4200-465 Porto, Portugal
* Correspondence: alexandra.galhano@ulusofona.pt

Abstract: A numerical technique was developed for solving nonlocal nonlinear stochastic delayed differential equations driven by fractional variable-order Brownian noise. Error analysis of the proposed technique was performed and discussed. The method was applied to the nonlocal stochastic fluctuations of the human body and the Nicholson's blowfly models, and its accuracy and computational time were assessed for different values of the nonlocal order parameters. A comparison with other techniques available in the literature revealed the effectiveness of the proposed scheme.

Keywords: fractional stochastic delayed differential equation; variable-order fractional Brownian noise; cubic spline interpolation; fractional calculus

MSC: 26A33; 34K37; 60H35; 65C30; 65D07; 60G22

Citation: Moghaddam, B.P.; Pishbin, M.; Mostaghim, Z.S.; Iyiola, O.S.; Galhano, A.; Lopes, A.M. A Numerical Algorithm for Solving Nonlocal Nonlinear Stochastic Delayed Systems with Variable-Order Fractional Brownian Noise. *Fractal Fract.* **2023**, *7*, 293. https://doi.org/10.3390/fractalfract7040293

Academic Editors: Palle Jorgensen and Ricardo Almeida

Received: 18 January 2023
Revised: 12 March 2023
Accepted: 27 March 2023
Published: 29 March 2023

1. Introduction

Fractional calculus (FC) deals with the differentiation and integration operators of arbitrary orders [1–3]. Over the last decades, FC has become globally recognized in nearly all fields due to its widespread usage, such as in mathematics [4–7], mechanics [8–10], physics [11,12], biology [13,14], and economics [15,16]. Fractional differential equations (FDEs) with and without noise are powerful mathematical tools for investigating phenomena in many applied sciences. The FDEs are studied in various branches of science, including chaotic oscillations [17,18], engineering [19,20], image processing [21,22], and epidemic models [23–25]. The existence and uniqueness studies involving FDEs were reviewed in [26,27]. In addition, many papers present distinct numerical techniques for various classes of FDEs, those including Chebyshev polynomials [28–30], finite difference [31], Hermite wavelet [32], Jacobi collocation [33], Legendre collocation [34], and others [35–37]. Recently, a novel exponential time differencing (ETD-RDP) method was developed by Iyiola et al. [38] to handle space-fractional reaction–diffusion systems with mixed and mismatched initial and boundary conditions for which regular numerical methods are unsuitable.

Variable-order fractional operators preserve memory and the hereditary properties of dynamical systems, while the constant-order fractional operators characterize memory with a uniform pattern [39,40]. Fractional differential equations of variable-order include those with classical operators, as well as others with short memory operators, which constitute a new kind of variable-order method [41–43]. Moreover, constant-order fractional operators are a special case (and probably the simplest one) of variable-order fractional ones.

The *variable-order fractional Brownian motion* (VOFBM) is expressed as a Gaussian process via the variable-order Hurst index [44]. The FDEs driven by VOFBM noise have

several usages, such as in physics [45], finance [46], and signal processing [47]. The VOFBM is defined as [44]:

$$\varpi^{H(t)}(t) = \frac{1}{\Gamma(H(t)+\frac{1}{2})}\int_0^t (t-\tau)^{H(t)-\frac{1}{2}}\varpi(\tau)d\tau, \quad \frac{1}{2} < H(t) < 1, \qquad t \geq 0. \tag{1}$$

In the follow-up, we assume that $(\Psi, \mathcal{F}, P)$ denotes a fixed probability space with normal filtration $(\mathcal{F}_t)_{t\geq 0}$.

There are distinct kinds of fractional uncertain differential equations [48]. In this paper, we studied the fractional stochastic delay differential equation driven by VOFBM (FSDDE-VOFBM), given by:

$$\begin{cases} {}^{C}\mathscr{D}^{\gamma}_{0,t}u(t) = G(t,u(t),u(t-\lambda)+M(t,u(t))\dfrac{d\varpi^{H(t)}(t)}{dt}, & t\in(0,T] \\ u(t) = \Theta(t), & t\in[-\lambda,0], \end{cases} \tag{2}$$

where $\gamma \in (\frac{1}{2}, 1)$ and ${}^{C}\mathscr{D}^{\gamma}_{0,t}u(t)$ denote the Caputo fractional derivative [49]:

$${}^{C}\mathscr{D}^{\gamma}_{0,t}u(t) = \frac{1}{\Gamma(b-\gamma)}\int_0^t \frac{u^{(b)}(\phi)}{(t-\phi)^{\gamma+1-b}}d\phi, \quad 0 \leq b-1 < \gamma \leq b \in \mathbb{N}, \tag{3}$$

where $\gamma \in \mathbb{R}^+$ is the order and $u^{(b)}(t)$ represents a smooth and continuously differentiable function on the interval $\Psi = [0, T]$. Additionally, $G \in \mathbb{C}(\Psi, \mathbb{R}, \mathbb{R})$, $M \in \mathbb{C}(\Psi, \mathbb{R})$, λ represents a time delay, $\Theta(t)$ stands for a function on the interval $t \in [-\lambda, 0]$ related to system history, and $\varpi(t)$ $(t \geq 0)$ is a Wiener's process.

There are several definitions of fractional derivative [50,51]. Commonly used formulations are the Grünwald–Letnikov, Riemann–Liouville and Caputo ones. In this paper, we adopted the Caputo fractional derivative. Indeed, it is the most frequently used in engineering and physics applications, since it allows traditional initial and boundary conditions to be included in the corresponding fractional equations, and the Caputo derivative of a constant is zero. Additionally, the Riemann–Liouville definition can be transformed into the Caputo one using an auxiliary power function. The Caputo derivative is an appropriate mean for modeling phenomena characterized by interactions with the past and nonlocal properties.

In this work, a numerical technique was developed for solving the nonlocal nonlinear FSDDE-VOFBM. An error analysis was performed and discussed. The effectiveness of the new method was assessed using some examples, for different values of the nonlocal order parameters. Therefore, the main novelty and contributions of the manuscript can be summarized as follows:

- An accurate and computationally efficient technique for solving FSDDE-VOFBM with Hurst index was proposed;
- A cubic spline interpolation method for time discretization was adopted;
- Error and convergence analysis of the suggested scheme was performed;
- The proposed numerical technique was applied to fractional stochastic dynamical systems and assessed from the perspective of statistical indicators of stochastic responses.

It should be mentioned that the method is valid for nonlocal nonlinear stochastic delayed differential equations using fractional variable-order Brownian noise and, thus, goes beyond other techniques [52,53], which focus on the existence and uniqueness of solutions for different classes of stochastic delay differential equations driven by fractional Brownian motion with the Hurst parameter $H > 1/2$.

The rest of this paper is divided into four sections. Section 2 proposes an explicit method based on cubic spline interpolation to discretize and solve the FSDDE-VOFBM (2). It describes an error analysis of the technique. Section 3 assesses the method accuracy, considering the nonlocal stochastic fluctuation of the human body and the Nicholson's blowfly model. Finally, Section 4 summarizes the main considerations.

2. Computational Implementation

An explicit approach for solving the FSDDE-VOFBM (2) was proposed, and error analysis was performed. In the follow-up we considered that $t_l = l\Delta$, with $\Delta = [\frac{T}{\varrho}]$ denoting an uniform step size and $l = \{0, 1, \ldots, \varrho\}$, with $\varrho \in \mathbb{N}$. The cubic spline $s_\varrho(\phi)$ is of the form

$$\frac{\mathrm{d}^b}{\mathrm{d}\phi^b}u(\phi) \approx s_\varrho(\phi) = \sum_{l=0}^{\varrho} N_{l,\varrho}(\phi)\frac{\mathrm{d}^b}{\mathrm{d}\phi^b}u_l + \sum_{l=0}^{\varrho} M_{l,\varrho}(\phi)\frac{\mathrm{d}^{b+1}}{\mathrm{d}\phi^b}u_{l+1}, \tag{4}$$

where the shape functions are stated as $N_{l,\varrho}(\phi)$ and $M_{l,\varrho}(\phi)$ in each interval $[t_l, t_{l+1}]$, for $1 \le l \le \varrho - 1$, given by

$$N_{l,\varrho}(\phi) = \begin{cases} \left(1 - \dfrac{2\phi - 2t_l}{t_l - t_{l+1}}\right)\left(\dfrac{\phi - t_{l+1}}{t_l - t_{l+1}}\right)^2, & t_{l-1} \le \phi \le t_l \\ \left(1 - \dfrac{2\phi - 2t_{l+1}}{t_{l+1} - t_l}\right)\left(\dfrac{\phi - t_l}{t_{l+1} - t_l}\right)^2, & t_l \le \phi \le t_{l+1} \\ 0, & \text{otherwise} \end{cases},$$

and

$$M_{l,\varrho}(\phi) = \begin{cases} (\phi - t_l)\left(\dfrac{\phi - t_{l+1}}{t_l - t_{l+1}}\right)^2, & t_{l-1} \le \phi \le t_l \\ (\phi - t_{l+1})\left(\dfrac{\phi - t_l}{t_{l+1} - t_l}\right)^2, & t_l \le \phi \le t_{l+1} \\ 0, & \text{otherwise} \end{cases}.$$

For $l = \{0, \varrho\}$, $N_{l,\varrho}(\phi)$ and $M_{l,\varrho}(\phi)$ are of the form

$$\begin{cases} N_{0,\varrho}(\phi) = \left(1 - \dfrac{2\phi - 2t_1}{t_1 - t_0}\right)\left(\dfrac{\phi - t_0}{t_1 - t_0}\right)^2, & t_0 \le \phi \le t_1 \\ N_{\varrho,\varrho}(\phi) = \left(1 - \dfrac{2\phi - 2t_\varrho}{t_\varrho - t_{\varrho+1}}\right)\left(\dfrac{\phi - t_{\varrho+1}}{t_\varrho - t_{\varrho+1}}\right)^2, & t_{\varrho-1} \le \phi \le t_\varrho \\ N_{0,\varrho}(\phi) = N_{\varrho,\varrho}(\phi) = 0, & \text{otherwise} \end{cases},$$

and

$$\begin{cases} M_{0,\varrho}(\phi) = (\phi - t_1)\left(\dfrac{\phi - t_0}{t_1 - t_0}\right)^2, & t_0 \le \phi \le t_1 \\ M_{\varrho,\varrho}(\phi) = (\phi - t_\varrho)\left(\dfrac{\phi - t_{\varrho+1}}{t_\varrho - t_{\varrho+1}}\right)^2, & t_{\varrho-1} \le \phi \le t_\varrho \\ M_{0,\varrho}(\phi) = M_{\varrho,\varrho}(\phi) = 0, & \text{otherwise} \end{cases}.$$

Therefore, we get

$$\begin{aligned} {}^C\mathscr{D}^\gamma_{0,t_\varrho}[u(t)] \quad &\approx \quad \left({}^C\mathscr{D}^\gamma_{0,t_\varrho}[u(t)]\right)_{approx} \\ &\equiv \quad \sum_{l=0}^{\varrho}\left(\int_{t_l}^{t_{l+1}} \frac{(t_\varrho - \zeta)^{b-1-\gamma}}{\Gamma(b-\gamma)} N_{l,\varrho}(\phi)\mathrm{d}\phi\right)\frac{\mathrm{d}^b}{\mathrm{d}\phi^b}u(t_l) \\ &+ \quad \sum_{l=0}^{\varrho}\left(\int_{t_l}^{t_{l+1}} \frac{(t_\varrho - \phi)^{b-1-\gamma}}{\Gamma(b-\gamma)} M_{l,\varrho}(\phi)\mathrm{d}\phi\right)\frac{\mathrm{d}^{b+1}}{\mathrm{d}\phi^{b+1}}u(t_l). \end{aligned} \tag{5}$$

and, after some calculations, we obtain

$${}^C\mathscr{D}^\gamma_{0,t_\varrho}[u(t)] \approx \sum_{l=0}^{\varrho}\frac{\Delta^{b-\gamma}}{\Gamma(b-\gamma+4)}\alpha_{l,\varrho}u_l^{(b)} + \sum_{l=0}^{\varrho}\frac{\Delta^{b-\gamma+1}}{\Gamma(b-\gamma+4)}\beta_{l,\varrho}u_l^{(b+1)}, \tag{6}$$

where

$$\alpha_{l,\varrho} = \begin{cases} -6(2\varrho+1+b-\gamma)(\varrho-1)^{b-\gamma+2} + \varrho^{b-\gamma} \times \Big((-6(b-\gamma)-18)\varrho^2 \\ \qquad +12\varrho^3 + (b-\gamma)^3 + 6(b-\gamma)^2 + 11(b-\gamma) + 6 \Big), & l = 0 \\ 6\Big((\varrho-l-1)^{b-\gamma+2}(2l-2\varrho-b+\gamma-1) \\ \qquad +(\varrho-l+1)^{b-\gamma+2}(2l-2\varrho-b+\gamma+1+4(\varrho-l)^{b-\gamma+3}) \Big), & 1 \le l \le \varrho-1 \\ 6(b-\gamma+1), & l = \varrho \end{cases},$$

and

$$\beta_{l,\varrho} = \begin{cases} -(6\varrho+2(b-\gamma))(\varrho-1)^{b-\gamma+2} + n^{b-\gamma+1} \times \\ \quad \Big(b-\gamma^2 + (-4\varrho+5)(b-\gamma) + 6(\varrho-1) \Big), & l = 0 \\ 2(3l-3\varrho-b+\gamma)(\varrho-l-1)^{b-\gamma+2} \\ \qquad -2(3l-3\varrho+b-\gamma)(\varrho-l+1)^{b-\gamma+2} - 8(\varrho-l)^{b-\gamma+2}(b-\gamma+3), & 1 \le l \le \varrho-1 \\ -2(b-\gamma), & l = \varrho \end{cases}.$$

Thus, we get the following proposition.

Proposition 1. *Let us consider the function $u(t) \in C^{b+4}(\Psi)$, $\gamma > 0$, and $\|u^{(b+4)}\|_\infty \le A$, with $A > 0$. Therefore, for (6), the truncated error $\mathcal{R}_\varrho = {}^{C}\mathscr{D}^{\gamma}_{0,t_\varrho}[u(t)] - \Big({}^{C}\mathscr{D}^{\gamma}_{0,t_\varrho}[u(t)]\Big)_{approx}$ is bounded, such that*

$$\mathbb{E}\Big[|\mathcal{R}_\varrho|\Big] \le \frac{nA}{4! \times 16\Gamma(b+1-\gamma)}\Delta^{b-\gamma+4}. \tag{7}$$

Proof. Assume the error function, $\mathscr{E}(t)$, defined by

$$\mathscr{E}_l(t) = u_l^{(m)}(t) - s_l(t) = \frac{u^{(b+4)}(\varphi_l)}{4!}(t-t_l)^2(t-t_{l+1})^2,\ l = 1,\dots,\varrho, \tag{8}$$

where $\varphi_l \in [t_l, t_{l+1}]$. Thus,

$$\begin{aligned} \mathbb{E}\Big[|\mathcal{R}_\varrho|\Big] &= \mathbb{E}\Big[\frac{1}{\Gamma(b-\gamma)}\int_{t_0}^{t_\varrho}(t_\varrho-\phi)^{b-\gamma-1}\|\mathscr{E}(\phi)\|_\infty d\phi\Big] \\ &= \frac{1}{\Gamma(b-\gamma)}\mathbb{E}\Big[\sum_{l=0}^{\varrho-1}\int_{t_l}^{t_{l+1}}(t_\varrho-\phi)^{b-\gamma-1}\left\|\frac{u^{(b+4)}(\varphi_l)}{4!}(\phi-t_l)^2(\phi-t_{l+1})^2\right\|_\infty d\phi\Big] \\ &\le \frac{Ah^4}{4! \times 16\Gamma(b-\gamma)}\sum_{l=0}^{\varrho-1}\int_{t_l}^{t_{l+1}}(t_\varrho-\phi)^{b-\gamma-1}d\phi \\ &\le B\Delta^{b-\gamma+4}, \end{aligned}$$

where

$$B = \frac{nA}{4! \times 16\Gamma(b+1-\gamma)}.$$

□

Hereafter, the proposed algorithm will be briefly denoted as "**CSM**-algorithm". It should be noted that, for solving the initial condition problems such as (2), we incorporated the **CSM**-algorithm with the finite differential quotient stated as:

$$u^{(b)}(t) = \frac{1}{\Delta^b}\sum_{s=0}^{b}(-1)^s \begin{pmatrix} b \\ s \end{pmatrix} u(t+(p-s)\Delta) + \mathcal{O}(\Delta). \tag{9}$$

3. Numerical Results and Discussion

We assess the computational effort and accuracy of the proposed method, using the *experimental convergence order* (ECO) and *expected mean absolute error* (EMAE), given by:

$$ECO_{ms} = \log_2\left(\frac{\|\bar{\mathscr{E}}_{2\varrho}\|_{ms}}{\|\bar{\mathscr{E}}_{\varrho}\|_{ms}}\right), \tag{10}$$

and

$$\|\bar{\mathscr{E}}_{\varrho}\|_{ms} = \frac{1}{\varrho}\sum_{l=1}^{\varrho}\left(\mathbb{E}\left[\|u_l^{\varrho} - u_{2l}^{2\varrho}\|^2\right]\right)^{\frac{1}{2}}, \tag{11}$$

where u_l^{ϱ} and $u_{2l}^{2\varrho}$ stand for the approximate values of $u(t_l)$, and ϱ denotes the quantity of mesh interior points. Numerical experiments were performed with the software package Maple V2019 on a processor Intel (R) Core (TM) i7-7500U @ 2.70 GHz.

The approximate solutions and CPU time obtained with the proposed **CSM**-algorithm were compared with the **IQM** [54] and **BSM** methods [55].

Example 1. *We considered the fractional stochastic fluctuation of the human body, described as an inverted pendulum under the action of a time-delayed restoring force:*

$$I\,{}^{C}\mathscr{D}_{0,t}^{2\gamma}\theta(t) + \phi\,{}^{C}\mathscr{D}_{0,t}^{\gamma}\theta(t) - mgl\sin\theta(t) = \tilde{\chi}(\theta(t-\lambda)) + \sqrt{2\widetilde{R}}\frac{d\varpi^{H(t)}(t)}{dt}, \tag{12}$$

where ${}^{C}\mathscr{D}_{0,t}^{2\gamma}u(t)$ *denotes the Caputo fractional derivative, with* $\gamma \in (\frac{1}{2}, 1)$*, and* $I = ml^2$ *and* mg *are the moment of inertia and the weight of the pendulum, respectively. Figure 1 illustrates the schematic diagram of this model. Assuming that the sway angle complies with* $\theta \ngeq 5^{\circ}$*, then we have*

$$\begin{cases} {}^{C}\mathscr{D}_{0,t}^{\gamma}u(t) = \kappa u(t) + \chi(u(t-\lambda)) + \sigma\dfrac{d\varpi^{H(t)}(t)}{dt}, & t \in (0, 10] \\ u(t) = 0.1, & t \in [-\lambda, 0], \end{cases} \tag{13}$$

where $\frac{1}{2} < \gamma, H(t) \leq 1$*,*

$$\chi(u(t-\lambda)) = \eta\tanh(u(t-\lambda)),$$

and $\kappa \approx \sqrt{mgl/2I}$*. Moreover, the delay is indicated as* λ*, the negative feedback coefficient is introduced as* η*, and* $\sigma = \sqrt{2\widetilde{R}}$ *is used for the value of the noise. Equation (13) was investigated for* $H(t) = \frac{1}{2}$ *and different values of* $\gamma \in (0, 1]$ *in [56].*

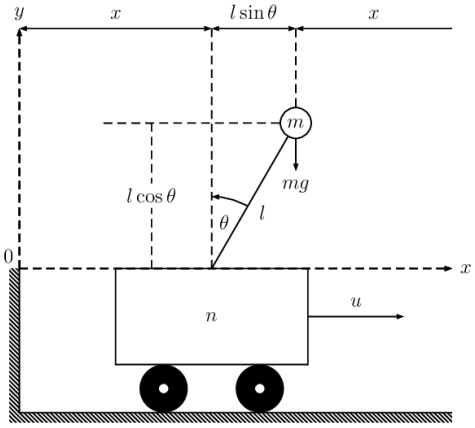

Figure 1. Inverted pendulum schematic chart stabilized by means of wain movements.

Figure 2 depicts the approximation of (13) for $\sigma = \{0, 0.01\}$ and $\gamma = \{0.55, 0.75, 0.95\}$, in $t \in [0, 10]$. Moreover, Table 1 compares $\|\bar{\mathscr{E}}_{\varrho}\|_{ms}$, ECO_{ms} and computational time obtained with the **IQM**- [54] and **CSM**-algorithms, for distinct values of Δ, $\gamma = \{0.25, 0.5, 0.7, 0.9\}$, and $t \in [0, 10]$. We verified that, for all values of γ, the errors yielded by the proposed method decrease as Δ diminishes. Table 2 lists the values of some statistical indicators (SIs) for several fractional orders, with$T = 10$. We verified that the values of the median and mean are equal for the fractional orders $\gamma = \{0.55, 0.75, 0.95\}$. This means that the diagram driven by 50 simulated paths at $T = 10$ is symmetric.

Table 1. Example 1: The values of $\|\bar{\mathscr{E}}_{\varrho}\|_{ms}$, ECO_{ms}, and CPU time (expressed in seconds) for (13) obtained with the **IQM**- [54] and **CSM**-algorithms for distinct choices of γ and Δ, with $\kappa = 1.58$, $\eta = -1.6$, $\sigma = 0.01$, $\lambda = 0.1$, and $H(t) = 0.95 - 0.02\,t$, in $t \in [0, 10]$.

		IQM-Algorithm [54]			**CSM-Algorithm**		
γ	Δ	$\|\bar{\mathscr{E}}_{\varrho}\|_{ms}$	ECO_{ms}	*CPU Time*	$\|\bar{\mathscr{E}}_{\varrho}\|_{ms}$	ECO_{ms}	*CPU Time*
0.55	0.02	2.18×10^{-4}	–	35.703	7.31×10^{-5}	–	26.344
	0.01	1.12×10^{-4}	0.96	151.516	6.31×10^{-6}	3.53	114.860
	0.005	6.04×10^{-5}	0.89	708.140	1.13×10^{-6}	2.48	494.953
0.75	0.02	2.49×10^{-4}	–	35.578	1.47×10^{-4}	–	25.719
	0.01	1.36×10^{-4}	0.87	147.922	1.01×10^{-5}	3.86	111.859
	0.005	7.39×10^{-5}	0.88	704.922	5.02×10^{-6}	2.32	490.843
0.95	0.02	5.65×10^{-4}	–	35.641	2.84×10^{-4}	–	25.438
	0.01	3.21×10^{-4}	0.85	151.937	1.60×10^{-5}	4.13	109.656
	0.005	1.57×10^{-4}	1.00	705.917	4.04×10^{-6}	1.98	499.797

Table 2. The approximated SI values concerning the 50 simulated paths for (13), with $\gamma = \{0.55, 0.75, 0.95\}$, $\kappa = 1.58$, $\eta = -1.6$, $\lambda = 0.1$, $\sigma = 0.01$, $H(t) = 0.95 - 0.02\,t$, and step size $\Delta = 0.01$, at $T = 10$.

SI	$\gamma = 0.55$	$\gamma = 0.75$	$\gamma = 0.95$
Mean	0.093	0.089	0.083
Median	0.093	0.089	0.083
First quartile	0.091	0.088	0.081
Third quartile	0.094	0.092	0.087
Kurtosis	2.350	2.582	2.944
Skewness	0.200	−0.038	−0.197
Standard deviation	2.268×10^{-3}	3.661×10^{-3}	5.975×10^{-3}
95% Confidence interval	[0.089, 0.097]	[0.083, 0.095]	[0.073, 0.093]

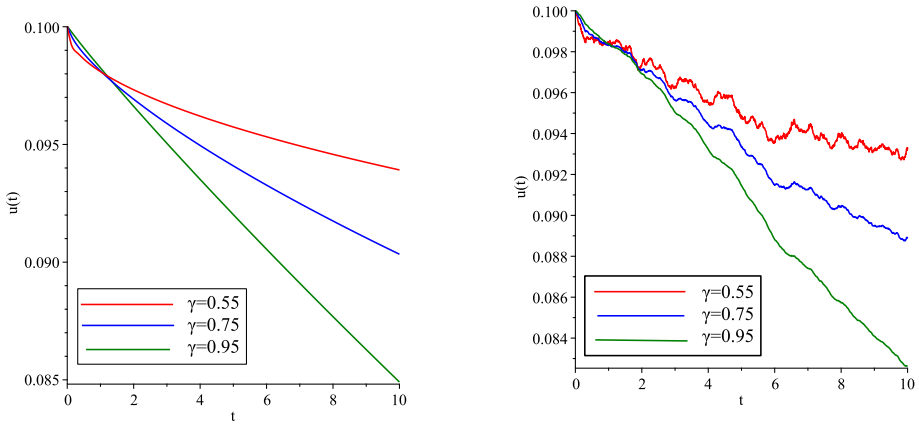

Figure 2. The time evolution of $u(t)$ for (12) with the proposed algorithm for $\kappa = 1.58$, $\eta = -1.6$, $\lambda = 0.1$, $\gamma = \{0.55, 0.75, 0.95\}$, $H(t) = 0.95 - 0.02t$, and $\Delta = 0.01$: (**left side**) $\sigma = 0$; (**right side**) $\sigma = 0.01$.

Example 2. *We considered the nonlinear fractional stochastic Nicholson's blowflies differential equation with time delay:*

$$\begin{cases} {}^{C}\mathscr{D}^{\gamma}_{0,t}u(t) = \kappa u(t-\lambda)\exp(-\mu u(t-\lambda)) \\ \qquad\qquad -\rho u(t) + \sigma\Big(u(t) - \mu^{-1}\ln\Big(\kappa\rho^{-1}\Big)\Big)\dfrac{d\varpi^{H(t)}(t)}{dt}, & t \in [0,10] \\ u(t) = 1.35\cos(3t), & t \in [-\lambda, 0] \end{cases}, \tag{14}$$

where $\frac{1}{2} < \gamma, H(t) \leq 1$, $u(t)$ *indicates the crowd size at the time instant* t, κ *represents peak per capita daily rate of egg production,* λ *denotes production time,* μ^{-1} *is the value at which the crowd multiplies at the peak rate,* ρ *is the adulthood per capita daily death rate, and* σ *introduces the publication coefficient. It should be noted that the model* (14)*, including non-stochastic and stochastic terms, was studied in [57,58].*

Figure 3 illustrates the approximated solutions of (14) for $\kappa = 9$, $\mu = 1$, $\lambda = 0.05$, $\rho = 2$, $H(t) = 0.6 + 0.2\exp(0.01t)$ and $\sigma = \{0, 5\}$ with different values of γ and step size $\Delta = 0.01$. We can observe the noise effect in Equation (14). Moreover, Figure 4 plots the approximation magnitudes of SIs of the 50 simulated paths for $\sigma = 5$, $\gamma = 0.55$ at $T = 10$.

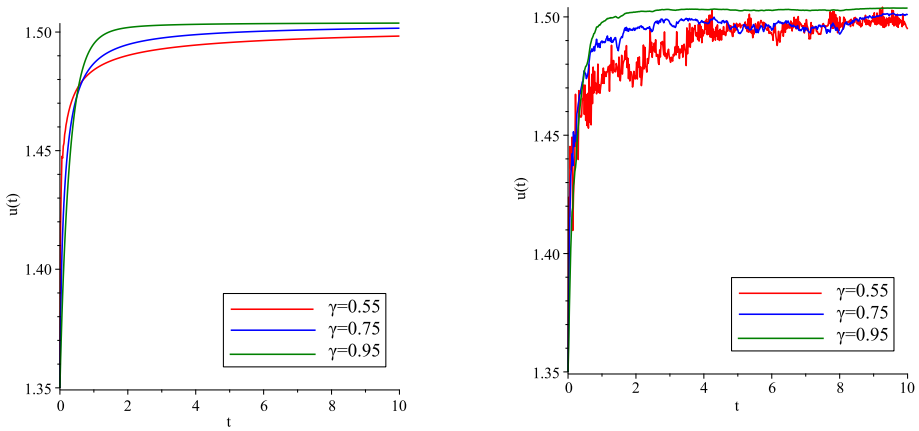

Figure 3. The time evolution of $u(t)$ for (14) with the proposed algorithm for $\kappa = 9$, $\mu = 1$, $\lambda = 0.05$, $\rho = 2$, $\gamma = \{0.55, 0.75, 0.95\}$, $H(t) = 0.6 + 0.2\exp(0.01t)$, and $\Delta = 0.01$: (**left side**) $\sigma = 0$; (**right side**) $\sigma = 5$.

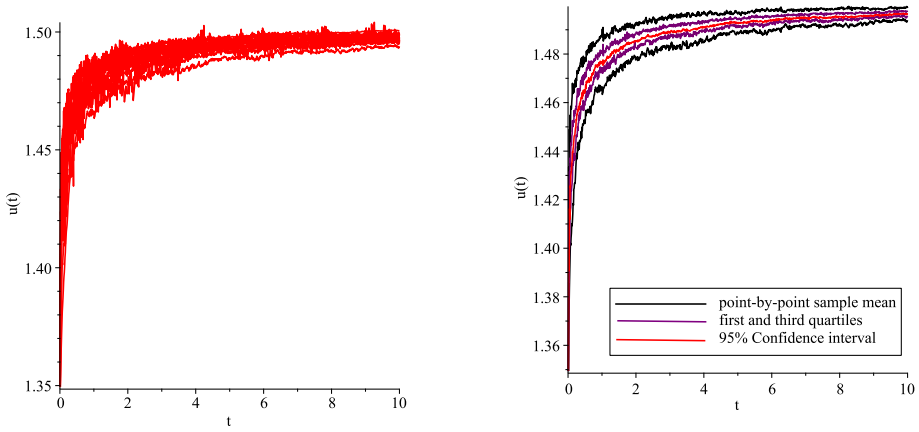

Figure 4. The time evolution of $u(t)$ (**left side**) and the SI values (**right side**) for (14) with the proposed algorithm, with $\kappa = 9$, $\mu = 1$, $\lambda = 0.05$, $\rho = 2$, $\sigma = 5$, $\gamma = 0.55$, $H(t) = 0.6 + 0.2\exp(0.01t)$ and $\Delta = 0.01$ over 50 simulated paths.

Table 3 summarizes $\|\bar{\mathscr{E}}_{\varrho}\|_{ms}$, ECO_{ms} and the computational time values of (14), obtained with the **BSM**- [55] and **CSM**-algorithms for $\gamma = \{0.55, 0.75, 0.95\}$, with $\Delta = \{0.02, 0.01, 0.005\}$ and $\lambda = 0.05$ in the time interval $t \in [0, 10]$. We verified that a more accurate approximation is obtained when reducing the step size. Table 4 presents the SI values for several γ cases, at $T = 10$. We verified that the diagram driven by 50 paths for $\gamma = \{0.55, 0.75, 0.95\}$ at $T = 10$ is symmetric. It should be noted that adopting $\sigma = 5$ corresponds to having data polluted by large random noise. Still, the stability of the proposed method was verified.

Finite difference methods are intuitive and easy to implement. However, the discretization schemes based on finite difference quotients do not necessarily increase convergence order by increasing the number of mesh points, just diminishing the error of the approximation. This limitation is mitigated by our method, which uses a discretization scheme based on cubic spline interpolation, with an implementation complexity similar to that of the finite difference method. The experimental convergence order of the proposed method is listed in Tables 1 and 3.

Table 3. Example 2: The values of $\|\bar{\mathscr{E}}_{\varrho}\|_{ms}$, ECO_{ms} and CPU time (expressed in seconds) for (14) obtained with the **BSM**- [55] and **CSM**-algorithms for different values of γ and Δ, with $\kappa = 9$, $\mu = 1$, $\lambda = 0.05$, $\rho = 2$, $\sigma = 5$, and $H(t) = 0.6 + 0.2\exp(0.01t)$, in $t \in [0, 10]$.

		BSM-Algorithm [55]			**CSM-Algorithm**		
γ	Δ	$\|\bar{\mathscr{E}}_{\varrho}\|_{ms}$	ECO_{ms}	*CPU Time*	$\|\bar{\mathscr{E}}_{\varrho}\|_{ms}$	ECO_{ms}	*CPU Time*
0.55	0.02	1.58×10^{-3}	–	10.140	9.54×10^{-4}	–	25.907
	0.01	9.88×10^{-4}	0.68	44.828	4.71×10^{-4}	1.02	114.094
	0.005	7.28×10^{-4}	0.44	194.265	8.68×10^{-5}	2.44	495.860
0.75	0.02	5.80×10^{-4}	–	9.937	3.98×10^{-4}	–	25.719
	0.01	2.91×10^{-4}	0.99	4.328	1.85×10^{-4}	1.10	115.375
	0.005	2.07×10^{-4}	0.49	191.828	5.43×10^{-5}	1.77	508.531
0.95	0.02	4.05×10^{-4}	–	10.687	3.96×10^{-4}	–	26.391
	0.01	2.26×10^{-4}	0.84	45.094	1.87×10^{-4}	1.08	120.328
	0.005	9.42×10^{-5}	1.26	185.047	5.89×10^{-5}	1.66	494.093

Table 4. The approximated SI values concerning the 50 simulated paths for (14), with $\gamma = \{0.55, 0.75, 0.95\}$, $\kappa = 9$, $\mu = 1$, $\lambda = 0.05$, $\rho = 2$, $\sigma = 5$, $H(t) = 0.6 + 0.2\exp(0.01t)$ and step size $\Delta = 0.01$, at $T = 10$.

SI	$\gamma = 0.55$	$\gamma = 0.75$	$\gamma = 0.95$
Mean	1.496	1.501	1.503
Median	1.496	1.501	1.503
First quartile	1.495	1.500	1.503
Third quartile	1.497	1.502	1.504
Kurtosis	3.145	2.670	2.567
Skewness	-0.834	-0.067	0.215
Standard deviation	1.490×10^{-3}	4.645×10^{-4}	5.198×10^{-5}
95% Confidence interval	$[1.493, 1.498]$	$[1.500, 1.502]$	$[1.503, 1.504]$

4. Conclusions

An explicit scheme based on cubic spline interpolation was proposed for numerically solving nonlocal FSDDE-VOFBM. The effectiveness of the method when applied to the nonlocal stochastic fluctuation of the human body and the Nicholson's blowfly models was investigated. Numerical experiments indicated the performance of the proposed method both in terms of accuracy and computational burden. The results also revealed the efficiency and feasibility of the algorithm for nonlinear stochastic delay systems. In future research, we will consider this technique for tackling models with distributed order fractional derivatives.

Author Contributions: Investigation, Methodology and Writing—original draft, B.P.M.; Software and Conceptualization, M.P. and Z.S.M.; Writing—review and editing, O.S.I.; visualization and supervision, A.G. and A.M.L. All authors have read and agreed to the published version of the manuscript.

Funding: This research received no external funding.

Data Availability Statement: Data sharing is not applicable to this article, as no datasets were generated or analyzed during the current study.

Conflicts of Interest: The authors declare no conflicts of interest.

References

1. Ortigueira, M.; Machado, J. Which derivative? *Fractal Fract.* **2017**, *1*, 3. [CrossRef]
2. Baleanu, D.; Agarwal, R.P. Fractional calculus in the sky. *Adv. Differ. Equations* **2021**, *2021*, 117. [CrossRef]
3. He, J.H. Fractal calculus and its geometrical explanation. *Results Phys.* **2018**, *10*, 272–276. [CrossRef]
4. Moghaddam, B.; Mendes Lopes, A.; Tenreiro Machado, J.; Mostaghim, Z. Computational scheme for solving nonlinear fractional stochastic differential equations with delay. *Stoch. Anal. Appl.* **2019**, *37*, 893–908. [CrossRef]
5. Tarasov, V.E. Mathematical Economics: Application of Fractional Calculus. *Mathematics* **2020**, *8*, 660. [CrossRef]
6. Milici, C.; Drăgănescu, G.; Machado, J.T. *Introduction to Fractional Differential Equations*; Springer: Berlin/Heidelberg, Germany, 2018; Volume 25.
7. Wang, K.J.; Shi, F. A New Perspective on the Exact Solutions of the Local Fractional Modified Benjamin–Bona–Mahony Equation on Cantor Sets. *Fractal Fract.* **2023**, *7*, 72. [CrossRef]
8. Szajek, K.; Sumelka, W.; Blaszczyk, T.; Bekus, K. On selected aspects of space-fractional continuum mechanics model approximation. *Int. J. Mech. Sci.* **2020**, *167*, 105287. [CrossRef]
9. Failla, G.; Zingales, M. Advanced materials modelling via fractional calculus: Challenges and perspectives. *Philos. Trans. R. Soc. A* **2020**, *378*, 20200050. [CrossRef]
10. Wu, F.; Zhang, H.; Zou, Q.; Li, C.; Chen, J.; Gao, R. Viscoelastic-plastic damage creep model for salt rock based on fractional derivative theory. *Mech. Mater.* **2020**, *150*, 103600. [CrossRef]
11. Kumar, D.; Baleanu, D. Fractional calculus and its applications in physics. *Front. Phys.* **2019**, *7*, 81. [CrossRef]
12. Goldfain, E. Fractional dynamics and the standard model for particle physics. *Commun. Nonlinear Sci. Numer. Simul.* **2008**, *13*, 1397–1404. [CrossRef]
13. Ghita, M.; Birs, I.R.; Copot, D.; Muresan, C.I.; Ionescu, C.M. Bioelectrical impedance analysis of thermal-induced cutaneous nociception. *Biomed. Signal Process. Control.* **2023**, *83*, 104678. [CrossRef]

14. Ghita, M.; Copot, D.; Ionescu, C.M. Lung cancer dynamics using fractional order impedance modeling on a mimicked lung tumor setup. *J. Adv. Res.* **2021**, *32*, 61–71. [CrossRef]
15. Tejado, I.; Valério, D.; Pérez, E.; Valério, N. Fractional calculus in economic growth modelling: The Spanish and Portuguese cases. *Int. J. Dyn. Control.* **2017**, *5*, 208–222. [CrossRef]
16. Farman, M.; Akgül, A.; Baleanu, D.; Imtiaz, S.; Ahmad, A. Analysis of fractional order chaotic financial model with minimum interest rate impact. *Fractal Fract.* **2020**, *4*, 43. [CrossRef]
17. Tavazoei, M.S.; Haeri, M.; Jafari, S.; Bolouki, S.; Siami, M. Some applications of fractional calculus in suppression of chaotic oscillations. *IEEE Trans. Ind. Electron.* **2008**, *55*, 4094–4101. [CrossRef]
18. Baleanu, D.; Sajjadi, S.S.; Jajarmi, A.; Defterli, Ö. On a nonlinear dynamical system with both chaotic and nonchaotic behaviors: A new fractional analysis and control. *Adv. Differ. Equations* **2021**, *2021*, 234. [CrossRef]
19. Zúñiga-Aguilar, C.; Gómez-Aguilar, J.; Escobar-Jiménez, R.; Romero-Ugalde, H. A novel method to solve variable-order fractional delay differential equations based in Lagrange interpolations. *Chaos Solitons Fract.* **2019**, *126*, 266–282. [CrossRef]
20. Iyiola, O.S.; Olayinka, O.G.; Mmaduabuchi, O. Analytical solutions of time-fractional models for homogeneous Gardner equation and non-homogeneous differential equations. *Alex. Eng. J.* **2016**, *55*, 1655–1659. [CrossRef]
21. Yang, Q.; Chen, D.; Zhao, T.; Chen, Y. Fractional calculus in image processing: A review. *Fract. Calc. Appl. Anal.* **2016**, *19*, 1222–1249. [CrossRef]
22. Ismail, S.M.; Said, L.A.; Radwan, A.G.; Madian, A.H.; Abu-ElYazeed, M.F. A novel image encryption system merging fractional-order edge detection and generalized chaotic maps. *Signal Process.* **2020**, *167*, 107280. [CrossRef]
23. Rihan, F.A.; Alsakaji, H.J. Dynamics of a stochastic delay differential model for COVID-19 infection with asymptomatic infected and interacting people: Case study in the UAE. *Results Phys.* **2021**, *28*, 104658. [CrossRef] [PubMed]
24. Iyiola, O.S.; Oduro, B.; Zabilowicz, T.; Iyiola, B.; Kenes, D. System of time fractional models for COVID-19: Modeling, analysis and solutions. *Symmetry* **2021**, *13*, 787. [CrossRef]
25. Iyiola, O.S.; Oduro, B.; Zabilowicz, T.; Iyiola, B.; Kenes, D. Analysis and solutions of generalized Chagas vectors re-infestation model of fractional order type. *Chaos Solitons Fractals* **2021**, *145*, 110797. [CrossRef]
26. Balachandran, K.; Kokila, J.; Trujillo, J. Existence of solutions of nonlinear fractional pantograph equations. *Acta Math. Sci.* **2013**, *33*, 712–720. [CrossRef]
27. Karakoç, F. Existence and uniqueness for fractional order functional differential equations with Hilfer derivative. *Differ. Equations Appl.* **2020**, *12*, 323–336. [CrossRef]
28. Dabiri, A.; Butcher, E.A. Numerical solution of multi-order fractional differential equations with multiple delays via spectral collocation methods. *Appl. Math. Model.* **2018**, *56*, 424–448. [CrossRef]
29. Heydari, M.H.; Mahmoudi, M.R.; Shakiba, A.; Avazzadeh, Z. Chebyshev cardinal wavelets and their application in solving nonlinear stochastic differential equations with fractional Brownian motion. *Commun. Nonlinear Sci. Numer. Simul.* **2018**, *64*, 98–121. [CrossRef]
30. Babaei, A.; Jafari, H.; Banihashemi, S. A collocation approach for solving time-fractional stochastic heat equation driven by an additive noise. *Symmetry* **2020**, *12*, 904. [CrossRef]
31. Mostaghim, Z.S.; Moghaddam, B.P.; Haghgozar, H.S. Computational technique for simulating variable-order fractional Heston model with application in US stock market. *Math. Sci.* **2018**, *12*, 277–283. [CrossRef]
32. Saeed, U.; ur Rehman, M. Hermite Wavelet Method for Fractional Delay Differential Equations. *J. Differ. Equations* **2014**, *2014*, 359093. [CrossRef]
33. Banihashemi, S.; Jafari, H.; Babaei, A. A stable collocation approach to solve a neutral delay stochastic differential equation of fractional order. *J. Comput. Appl. Math.* **2022**, *403*, 113845. [CrossRef]
34. Doha, E.H.; Abdelkawy, M.A.; Amin, A.Z.M.; Lopes, A.M. Shifted fractional Legendre spectral collocation technique for solving fractional stochastic Volterra integro-differential equations. *Eng. Comput.* **2021**, *38*, 1363–1373. [CrossRef]
35. Bhrawy, A.H.; Taha, T.M.; Machado, J.A.T. A review of operational matrices and spectral techniques for fractional calculus. *Nonlinear Dyn.* **2015**, *81*, 1023–1052. [CrossRef]
36. Hassani, H.; Avazzadeh, Z.; Machado, J. Numerical approach for solving variable-order space–time fractional telegraph equation using transcendental Bernstein series. *Eng. Comput.* **2020**, *36*, 867–878. [CrossRef]
37. Hassani, H.; Machado, J.; Avazzadeh, Z. An effective numerical method for solving nonlinear variable-order fractional functional boundary value problems through optimization technique. *Nonlinear Dyn.* **2019**, *97*, 2041–2054. [CrossRef]
38. Iyiola, O.S.; Wade, B.A. Exponential integrator methods for systems of non-linear space-fractional models with super-diffusion processes in pattern formation. *Comput. Math. Appl.* **2018**, *75*, 3719–3736. [CrossRef]
39. Lorenzo, C.F.; Hartley, T.T. Variable order and distributed order fractional operators. *Nonlinear Dyn.* **2002**, *29*, 57–98. [CrossRef]
40. Patnaik, S.; Hollkamp, J.P.; Semperlotti, F. Applications of variable-order fractional operators: A review. *Proc. R. Soc. A* **2020**, *476*, 20190498. [CrossRef]
41. Baleanu, D.; Wu, G.C. Some further results of the laplace transform for variable–order fractional difference equations. *Fract. Calc. Appl. Anal.* **2019**, *22*, 1641–1654. [CrossRef]
42. Wu, G.C.; Luo, M.; Huang, L.L.; Banerjee, S. Short memory fractional differential equations for new memristor and neural network design. *Nonlinear Dyn.* **2020**, *100*, 3611–3623. [CrossRef]

43. Ma, C.Y.; Shiri, B.; Wu, G.C.; Baleanu, D. New fractional signal smoothing equations with short memory and variable order. *Optik* **2020**, *218*, 164507. [CrossRef]
44. Sheng, H.; Sun, H.; Chen, Y.Q.; Qiu, T. Synthesis of multifractional Gaussian noises based on variable-order fractional operators. *Signal Process.* **2011**, *91*, 1645–1650. [CrossRef]
45. Shahnazi-Pour, A.; Moghaddam, B.P.; Babaei, A. Numerical simulation of the Hurst index of solutions of fractional stochastic dynamical systems driven by fractional Brownian motion. *J. Comput. Appl. Math.* **2021**, *386*, 113210. [CrossRef]
46. Corlay, S.; Lebovits, J.; Véhel, J.L. Multifractional stochastic volatility models. *Math. Financ.* **2014**, *24*, 364–402. [CrossRef]
47. Sheng, H.; Chen, Y.Q.; Qiu, T. *Fractional Processes and Fractional-Order Signal Processing: Techniques and Applications*; Springer Science & Business Media: Cham, Switzerland, 2011.
48. Wu, G.C.; Wei, J.L.; Luo, C.; Huang, L.L. Parameter estimation of fractional uncertain differential equations via Adams method. *Nonlinear Anal. Model. Control.* **2022**, *27*, 413–427. [CrossRef]
49. Samko, S.G.; Kilbas, A.A.; Marichev, O.I. *Fractional Integrals and Derivatives: Theory and Applications*; Gordon & Breach Sci. Publishers: London, UK, 1993.
50. De Oliveira, E.C.; Tenreiro Machado, J.A. A review of definitions for fractional derivatives and integral. *Math. Probl. Eng.* **2014**, *2014*, 238459. [CrossRef]
51. Valério, D.; Ortigueira, M.D.; Lopes, A.M. How many fractional derivatives are there? *Mathematics* **2022**, *10*, 737. [CrossRef]
52. Lv, J.; Yang, X. Nonlocal fractional stochastic differential equations driven by fractional Brownian motion. *Adv. Differ. Equations* **2017**, *2017*, 198. [CrossRef]
53. El-Borai, M.M.; El-Nadi, K.E.S.; Fouad, H.A. On some fractional stochastic delay differential equations. *Comput. Math. Appl.* **2010**, *59*, 1165–1170. [CrossRef]
54. Mostaghim, Z.S.; Moghaddam, B.P.; Haghgozar, H.S. Numerical simulation of fractional-order dynamical systems in noisy environments. *Comput. Appl. Math.* **2018**, *37*, 6433–6447. [CrossRef]
55. Moghaddam, B.P.; Mostaghim, Z.S.; Hashemi-Zadeh, E. Computational Method for Fractional-Order Stochastic Delay Differential Equations. *J. New Res. Math.* **2020**, *6*, 19–32.
56. Boulet, J.; Balasubramaniam, R.; Daffertshofer, A.; Longtin, A. Stochastic two-delay differential model of delayed visual feedback effects on postural dynamics. *Philos. Trans. R. Soc. A: Math. Phys. Eng. Sci.* **2010**, *368*, 423–438. [CrossRef] [PubMed]
57. Wang, W.; Chen, W. Persistence and extinction of Markov switched stochastic Nicholson's blowflies delayed differential equation. *Int. J. Biomath.* **2020**, *13*, 2050015. [CrossRef]
58. Huang, C.; Yang, X.; Cao, J. Stability analysis of Nicholson's blowflies equation with two different delays. *Math. Comput. Simul.* **2020**, *171*, 201–206. [CrossRef]